JPE 19-1-9

https://doi.org/10.6113/JPE.2019.19.1.89
ISSN(Print): 1598-2092 / ISSN(Online): 2093-4718

Unbalance Control Strategy of Boost Type Three-Phase to Single-Phase Matrix Converters Based on Lyapunov Function

Yu-xiang Xu†, Hong-juan Ge*, and Hai Guo*

†,*Nanjing University of Aeronautics and Astronautics, Nanjing, China

Abstract

This paper analyzes the input side performance of a conventional three-phase to single-phase matrix converter (3-1MC). It also presents the input-side waveform quality under this topology. The suppression of low-frequency input current harmonics is studied using the 3-1MC plus capacitance compensation unit. The constraint between the modulation function of the output and compensation sides is analyzed, and the relations among the voltage utilization ratio and the output compensation capacitance, filter capacitors and other system parameters are deduced. For a 3-1MC without large-capacity energy storage, the system performance is susceptible to input voltage imbalance. This paper decouples the inner current of the 3-1MC using a Lyapunov function in the input positive and negative sequence bi-coordinate axes. Meanwhile, the outer loop adopts a voltage-weighted synthesis of the output and compensation sides as a cascade of control objects. Experiments show that this strategy suppresses the low-frequency input current harmonics caused by input voltage imbalance, and ensures that the system maintains good static and dynamic performances under input-unbalanced conditions. At the same time, the parameter selection and debugging methods are simple.

Key words: Lyapunov function, Matrix converter, Positive and negative sequence, Unbalance, Weighted synthesis

I. INTRODUCTION

The matrix converter (MC) is a kind of "green converter" that has the advantages of low harmonic pollution, an adjustable input power factor, a bidirectional energy flow, and a high-power density. Based on these excellent attributes, it has received a lot of attention from scholars.

The three-phase to single-phase matrix converter (3-1MC) is a special form of the traditional M-phase to N-phase matrix converter. With the development of industrial technology, the 3-1MC has been used more and more as a special topology in matrix converter applications, such as battery charge and discharge management [2], micro-grid and distributed power grid interfaces [3], [4], wireless energy transmission [5], wind power [6], [7], and high-frequency induction heating [8]. The above research results show that the 3-1MC has good application prospects in single-phase power consumption. In this paper, the single-phase ripple power at the output side of the conventional 3-1MC topology directly affects the performance of the input side. The authors of [4], [9]-[12] propose a class of power compensation strategies for different types of 3-1MC topologies to suppress the impact of output pulsating power on system performance. The above methods make the double-frequency output ripple power form a loop on the output side and not couple to the input side. Although having no large-capacity DC side energy storage link brings a higher power density in practical applications, the input voltage imbalance and other anomalies directly affect the input and output performances of the matrix converter through the bidirectional switches, which results in input current and output voltage distortions. At present, research on control strategies for improving system performance under input imbalance is mainly focused on the three-phase to three-phase matrix converter (3-3MC) topology [13], [14]. The authors of [13] proposed an improved voltage synthesis control strategy to improve the quality of the 3-3MC input current and its output voltage waveforms. The authors of

Manuscript received May 29, 2018; accepted Sep. 15, 2018
Recommended for publication by Associate Editor Liqiang Yuan.
†Corresponding Author: keyan_xyx@163.com
Tel: +86-025-84896005, Nanjing Univ. of Aeronautics and Astronautics
*Nanjing University of Aeronautics and Astronautics, China

[14] proposed the use a proportional-integral resonance (PIR) regulator instead of the traditional proportional-integral (PI) regulator to suppress the low frequency ripple in the active power, which improved the quality of the input side current waveform. The authors of [15] proposed using a resonant controller to adjust the input current and active power values to eliminate the input current harmonics and to improve the output waveform. The unbalanced control strategy mentioned above covers matrix converters in the buck mode. However, the voltage boosting type is studies in this paper. Therefore, the voltage synthesis method described in [13] cannot be used to suppress the low-frequency harmonics in the input current. The parameter selection and discretization of the resonant converters in [14], [15] are more complex than a PI controller can handle. Since the 3-1MC can still be equivalent to a virtual rectification topology with a virtual inverter, the unbalanced control strategy of voltage-source pulse width modulation (PWM) rectifiers and inverters can provide ideas for the 3-1MC imbalance [16].

Therefore, in order to simultaneously determine the impact of output power pulsation and an unbalanced input on system performance, this paper studies the influence of the 3-1MC input imbalance on the input active and reactive powers, and derives the expressions of control equations under the positive and negative sequence double *dq* rotation axes based on the Lyapunov function method. Using the topologies in [10], [11] to eliminate the low-frequency harmonic components in the input current caused by unbalance, the use of the Lyapunov function theory is proposed to separate the active and reactive powers on the input side. The control improves the control effect of the single grid-side current feedback control strategy under a single rotating coordinate axis. Simultaneously, the system parameter setting is simplified, and the input and output performances under an unbalanced input are improved. Finally, the effectiveness and feasibility of the proposed control strategy are verified by simulation and experimental results.

II. Power Compensation Principle

A. Input Waveform Quality Analysis

A boost-type 3-1MC topology based on capacitance for power compensation was studied in [11], as shown in Fig. 1. The topology includes an input inductor L, a bidirectional switch S_{ij} (i = a, b, c; j = u, v, w), a load R_L, an output filter capacitor C_f, and a compensation capacitor C_c. The conventional 3-1MC topology does not include the compensation unit C_c or the bidirectional switches S_{av}, S_{bv} and S_{cv} in Fig. 1. The output side single-phase voltage and fundamental current wave expression are expressed as:

$$\begin{cases} i_o = I_o \cos(\omega_o t + \delta_1) \\ u_o = U_o \cos(\omega_o t + \delta_1 + \delta) = I_o |Z_L| \cos(\omega_o t + \delta_1 + \delta) \\ |Z_L| = \dfrac{R_L}{\sqrt{(R_L C_f \omega_o)^2 + 1}} \end{cases} \tag{1}$$

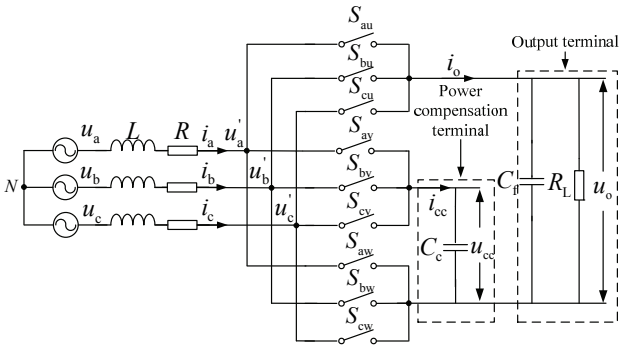

Fig. 1. Pulsating power compensation unit of the 3-1MC topology.

where, ω_o denotes the output voltage angular frequency, while U_o and I_o denote the output voltage and current amplitude, respectively. δ is the phase difference between the output voltage and the current, δ_1 is the output side current initial phase, and $|Z_L|$ is the output side impedance.

The expression for the output power from the above equation is:

$$P_o = u_o i_o = \underbrace{\frac{U_o I_o \cos(\delta)}{2}}_{\overline{P}_o} + \underbrace{\frac{U_o I_o \cos(2\omega_o t + 2\delta_1 + \delta)}{2}}_{\tilde{P}_o} \tag{2}$$

where, $\overline{P}_o$ and $\tilde{P}_o$ denote the constant and pulsating output powers, respectively.

Assuming the input is a symmetrical three-phase sinusoidal voltage, its expression is:

$$\begin{cases} u_a = U_i \cos(\omega_i t) \\ u_b = U_i \cos(\omega_i t - 2\pi/3) \\ u_c = U_i \cos(\omega_i t + 2\pi/3) \end{cases} \tag{3}$$

From the above equation, when the output is single-phase AC, in addition to the constant power in the output power, there is a pulsating power with twice the output frequency. Neglecting the system loss, according to the principle of the conservation of the instantaneous power of the input and output, in addition to the fundamental wave, the input three-phase current must contain harmonic components related to the output frequency. Ignoring the high-frequency harmonics in the input current, assume that the three-phase input current is:

$$\begin{cases} i_a = I_i \cos(\omega_i t + \varphi_1) - I_2 \cos(\omega_2 t + \varphi_2) - I_3 \cos(\omega_3 t + \varphi_3) \\ i_b = I_i \cos(\omega_i t + \varphi_1 - \frac{2}{3}\pi) - I_2 \cos(\omega_2 t + \varphi_2 - \frac{2}{3}\pi) - I_3 \cos(\omega_3 t + \varphi_3 + \frac{2}{3}\pi) \\ i_c = I_i \cos(\omega_i t + \varphi_1 + \frac{2}{3}\pi) - I_2 \cos(\omega_2 t + \varphi_2 + \frac{2}{3}\pi) - I_3 \cos(\omega_3 t + \varphi_3 - \frac{2}{3}\pi) \end{cases} \tag{4}$$

where, I_i denotes the amplitude of the fundamental current, φ_1 denotes the initial phase of the fundamental wave current, φ_2 and φ_3 denote the initial phases of the harmonic currents of ω_2 and ω_3 in the input current, I_2 and I_3 denote the amplitudes of the harmonics of ω_2 and ω_3 in the input current, and the harmonic current amplitude is assumed to

satisfy: $I_2 = I_3$.

The expression for the input power P_i can be obtained from Eqns. (3) and (4):

$$P_i = \frac{3}{2}U_i I_i \cos\varphi_1 - \frac{3}{2}U_i I_2 \cos[(\omega_1 - \omega_2)t + \varphi_2] - \frac{3}{2}U_i I_3 \cos[(\omega_1 + \omega_3)t - \varphi_3] \quad (5)$$

Ignoring the system loss, according to the principle that the input and output power are approximately equal, the frequency of the harmonics ω_2、ω_3 in the upper form are calculated according to the method of undetermined coefficients:

$$\begin{cases} \omega_2 = 2\omega_o + \omega_i \\ \omega_3 = 2\omega_o - \omega_i \end{cases} \quad (6)$$

For the upper formula there is a harmonic in the input current of ω_2 and ω_3, which is related to the input and output voltage frequencies ω_1 and ω_o. In addition, the low frequency harmonics are hard to eliminate via a low pass filter.

B. Theoretical Derivation of Compensation Function Implementation

To facilitate the analysis of the compensation function implementation process of the 3-1MC, the topology in Fig. 1 is equivalent to the virtual AC-DC-AC circuit structure shown in Fig. 2. In addition, the expressions of the compensation-side current modulation function ξ_c and the output-side current modulation function ξ_m are separately set as:

$$\begin{cases} \xi_m = M_m \cos(\omega_o t + \delta_1) \\ \xi_c = M_c \cos(\omega_o t + \delta_2) \end{cases} \quad (7)$$

where, M_m denotes the modulation coefficient of the output-side current modulation function, and M_c denotes the modulation coefficient of the compensation-side current modulation function. δ_2 is the initial phase of the compensation-side current modulation function.

The compensation side current i_{cc} and the voltage expressions u_{cc} are:

$$\begin{cases} i_{cc} = I_{cc}\cos(\omega_o t + \delta_2) \\ u_{cc} = U_{cc}\sin(\omega_o t + \delta_2) = I_{cc}|Z_{cc}|\sin(\omega_o t + \delta_2) \\ |Z_{cc}| = \dfrac{1}{\omega_o C_c} \end{cases} \quad (8)$$

where, I_{cc} denotes the amplitude of the compensation side current, U_{cc} denotes the amplitude of the fundamental voltage, and $|Z_{cc}|$ is the capacitor reactance.

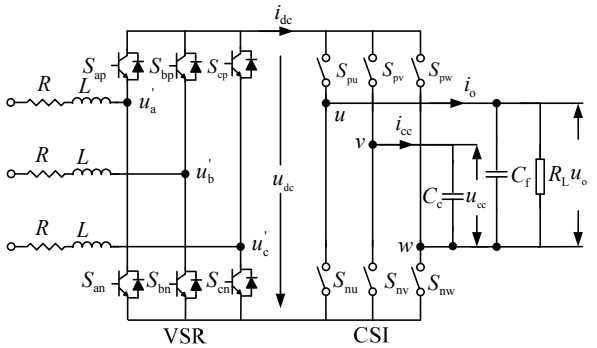

Fig. 2. Equivalent AC-DC-AC topology of a 3-1MC.

The compensation side and output total power expressions are:

$$\begin{cases} P_{cc} = u_{cc} i_{cc} = \dfrac{I_{cc}^2 |Z_{cc}|}{2}\sin(2\omega_o t + 2\delta_2) \\ P_{all} = P_{cc} + P_o \end{cases} \quad (9)$$

If the input is the three-phase symmetry current, the input power P_i is constant. It follows from (9) that the total output power P_{all} should also be constant. In this case, the output fluctuating power $\tilde{P}_o$ is cancelled by the power P_{cc} of the compensation side.

$$\begin{cases} \delta_2 = \delta_1 + \dfrac{\delta}{2} - \dfrac{\pi}{4} \\ \dfrac{I_o}{I_{cc}} = \dfrac{M_m}{M_c} = k_1 = \sqrt{\dfrac{|Z_{cc}|}{|Z_L|}} \end{cases} \quad (10)$$

C. System Voltage Utilization Analysis

The relation between the virtual bus voltage u_{dc} and the input voltage amplitude U_i in the AC-DC-DC topology of the virtual rectification and virtual inversion (shown in Fig. 2) is given in (11):

$$u_{dc} \geq \sqrt{3}U_i \quad (11)$$

The phase angle δ between the output voltage u_o and the current i_o is ignored, and the relationship between the voltage amplitude U_o at the output side and the virtual bus voltage u_{dc} is:

$$U_o = \frac{2u_{dc}}{M_m} \geq \frac{\sqrt{12}U_i}{M_m} \quad (12)$$

To obtain the maximum voltage utilization of the system, the zero-vector time of the output virtual inverter stage is minimized. For the sake of simplifying the derivation process, the phase angle of the initial current δ_1 in (7) is taken as zero. Then the current modulation function in (7) must satisfy the following constraint relationship:

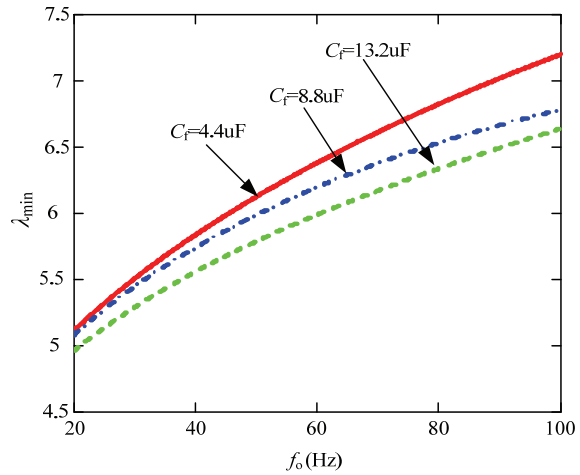

Fig. 3. Effect of the output filter capacitor C_f on the system minimum voltage utilization λ_{min}.

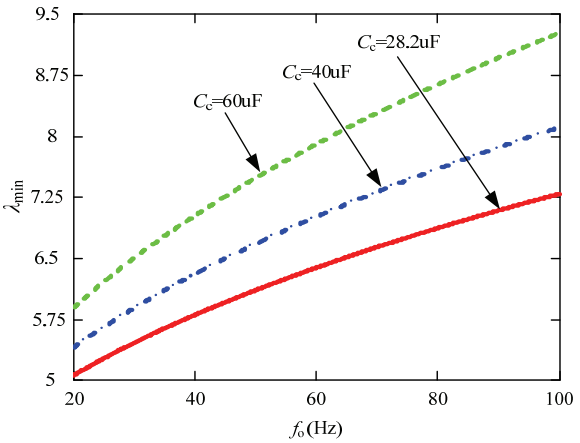

Fig. 4. Influence of different compensation capacitors C_c on the system minimum voltage utilization λ_{min}.

$$|\xi_m|+|\xi_c| = M_m|\cos(\omega_0 t+\delta_1)|+M_c|\cos(\omega_0 t+\delta_2)| \le M_m\sqrt{\left[1+k_1\cos(\delta/2-\pi/4)\right]^2+\left[k_1\sin(\delta/2-\pi/4)\right]^2} \le 1 \quad (13)$$

From (13), the maximum value of the current modulation coefficient M_m at the output side is:

$$M_{m\_max} = \frac{1}{\sqrt{\left[1+k_1\cos(\delta/2-\pi/4)\right]^2+\left[k_1\sin(\delta/2-\pi/4)\right]^2}} \quad (14)$$

Therefore, the 3-1MC voltage utilization λ expression shown in Fig. 1 is:

$$\lambda = \frac{U_o}{U_i} \ge \frac{\sqrt{12}}{M_m} \ge \sqrt{12}\sqrt{\left[1+k_1\cos(\delta/2-\pi/4)\right]^2+\left[k_1\sin(\delta/2-\pi/4)\right]^2} \quad (15)$$

The system parameters are set as follows:

1) The single-phase load $R_L = 100\Omega$.

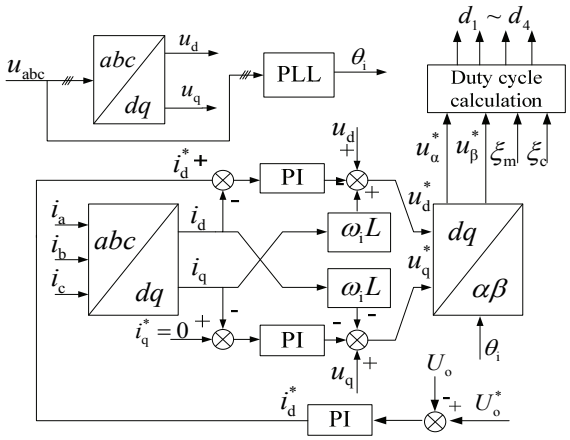

Fig. 5. Single grid-side current feedback loop control diagram of a 3-1MC.

2) The output filter capacitor $C_f = 4.4\text{uF}$.

3) The compensation capacitor $C_c = 28.2\text{uF}$.

Figs. 3 and 4 show the relationships among λ_{min} and the system parameters.

From Figs. 3 and 4, it can be seen that the topology studied in this paper is a boost matrix converter. The minimum voltage utilization λ_{min} of the system is related to the compensation capacitor C_c, and it is affected by the output-side filter capacitor C_f. It can be seen from Fig. 3 that when the value of the output side filter capacitor C_f changes and the other system parameters remain unchanged, the minimum voltage utilization λ_{min} of the system decreases with an increase of the filter capacitor C_f at the same output frequency. It can be seen from Fig. 4 that when the value of the compensation side capacitor C_c changes and the other system parameters remain unchanged, the minimum voltage utilization λ_{min} of the system increases with an increase of the compensation side capacitor C_c at the same output frequency. When compared with the traditional 3-3MC voltage utilization rate of no higher than 0.866, the proposed 3-1MC has a very high step-up ratio, which is very suitable for single-phase power consumption with amplitude step-up requirements.

III. 3-1MC Control Strategy Under an Unbalanced Input

A. Insufficient Single Grid-Side Current Feedback Control Strategy

The 3-1MC inner loop control under a three-phase voltage balanced input often adopts the single grid-side current feedback control strategy, whose control block diagram is shown in Fig. 5. This control strategy adopts a single current inner loop control. After the output voltage amplitude U_o is

adjusted by the PI regulator, the *dq* axis current components i_{d}^{*} and i_{q}^{*} of the given inner loop are output, and double closed loop control under a balanced input is realized.

When the input is a three-phase unbalanced voltage, assuming that the input is a three-phase asymmetrical current, this current only contains the fundamental component and no zero-sequence component. Then the input current is the sum of the positive sequence and negative sequence currents. As shown in (16):

$$\begin{aligned} i=\begin{bmatrix} i_{\mathrm{a}} \\ i_{\mathrm{b}} \\ i_{\mathrm{c}} \end{bmatrix}=\begin{bmatrix} i_{\mathrm{a}}^{\mathrm{p}} \\ i_{\mathrm{b}}^{\mathrm{p}} \\ i_{\mathrm{c}}^{\mathrm{p}} \end{bmatrix}+\begin{bmatrix} i_{\mathrm{a}}^{\mathrm{n}} \\ i_{\mathrm{b}}^{\mathrm{n}} \\ i_{\mathrm{c}}^{\mathrm{n}} \end{bmatrix}=&I^{\mathrm{p}}\begin{bmatrix} \cos(\omega_{\mathrm{l}}\mathrm{t}+\varphi_{\mathrm{p}}) \\ \cos(\omega_{\mathrm{l}}\mathrm{t}-\dfrac{2\pi}{3}+\varphi_{\mathrm{p}}) \\ \cos(\omega_{\mathrm{l}}\mathrm{t}+\dfrac{2\pi}{3}+\varphi_{\mathrm{p}}) \end{bmatrix} \\ &+I^{\mathrm{n}}\begin{bmatrix} \cos(\omega_{\mathrm{l}}\mathrm{t}+\varphi_{\mathrm{n}}) \\ \cos(\omega_{\mathrm{l}}\mathrm{t}+\dfrac{2\pi}{3}+\varphi_{\mathrm{n}}) \\ \cos(\omega_{\mathrm{l}}\mathrm{t}-\dfrac{2\pi}{3}+\varphi_{\mathrm{n}}) \end{bmatrix} \end{aligned} \tag{16}$$

where, $i_{\mathrm{a}}^{\mathrm{p}}$、$i_{\mathrm{b}}^{\mathrm{p}}$、$i_{\mathrm{c}}^{\mathrm{p}}$ denote the input current positive sequence components, $i_{\mathrm{a}}^{\mathrm{n}}$、$i_{\mathrm{b}}^{\mathrm{n}}$、$i_{\mathrm{c}}^{\mathrm{n}}$ denote the input current negative sequence components, and I^{p} and I^{n} denote input current positive and negative sequence amplitudes, respectively. φ_{p} and φ_{n} denote the initial phase of the positive and negative sequence components of the input current, respectively.

The expression of the *abc-dq* transformation of the three-phase to two-phase positive-sequence rotation axis transformation is:

$$T_{\mathrm{abc/dq}}^{\mathrm{p}}=\frac{2}{3}\begin{bmatrix} \cos\left(\omega_{\mathrm{l}}\mathrm{t}+\varphi_{\mathrm{p}}\right) & \cos\left(\omega_{\mathrm{l}}\mathrm{t}+\varphi_{\mathrm{p}}-\dfrac{2}{3}\pi\right) & \cos\left(\omega_{\mathrm{l}}\mathrm{t}+\varphi_{\mathrm{p}}+\dfrac{2}{3}\pi\right) \\ -\sin\left(\omega_{\mathrm{l}}\mathrm{t}+\varphi_{\mathrm{p}}\right) & -\sin\left(\omega_{\mathrm{l}}\mathrm{t}+\varphi_{\mathrm{p}}-\dfrac{2}{3}\pi\right) & -\sin\left(\omega_{\mathrm{l}}\mathrm{t}+\varphi_{\mathrm{p}}+\dfrac{2}{3}\pi\right) \end{bmatrix} \tag{17}$$

If the system adopts single grid-side current control, the input current positive sequence and negative sequence components are transformed under the positive sequence rotation *dq* coordinate axis as shown in (18) and (19), where the angular velocity of the positive and negative rotation *dq* axes is ω_{l}, the direction of rotation is reversed, and the initial positive and negative phases are φ_{p} and φ_{n}, respectively.

$$i_{\mathrm{dq}}^{\mathrm{p}}=T_{\mathrm{abc/dq}}^{\mathrm{p}}\begin{bmatrix} i_{\mathrm{a}}^{\mathrm{p}} \\ i_{\mathrm{b}}^{\mathrm{p}} \\ i_{\mathrm{c}}^{\mathrm{p}} \end{bmatrix}=I^{\mathrm{p}}\begin{bmatrix} 1 \\ 0 \end{bmatrix} \tag{18}$$

$$i_{\mathrm{dq}}^{\mathrm{n'}}=T_{\mathrm{abc/dq}}^{\mathrm{p}}\begin{bmatrix} i_{\mathrm{a}}^{\mathrm{n}} \\ i_{\mathrm{b}}^{\mathrm{n}} \\ i_{\mathrm{c}}^{\mathrm{n}} \end{bmatrix}=I^{\mathrm{n}}\begin{bmatrix} \cos(2\omega_{\mathrm{l}}\mathrm{t}+\varphi_{\mathrm{p}}+\varphi_{\mathrm{n}}) \\ -\sin(2\omega_{\mathrm{l}}\mathrm{t}+\varphi_{\mathrm{p}}+\varphi_{\mathrm{n}}) \end{bmatrix} \tag{19}$$

The total expression of the three-phase unbalanced current input in the positive-sequence *dq* rotation axis transformation is the sum of (18) and (19):

$$i_{\mathrm{dq}}=\begin{bmatrix} i_{\mathrm{d}} \\ i_{\mathrm{q}} \end{bmatrix}=\begin{bmatrix} i_{\mathrm{d}}^{\mathrm{p}} \\ i_{\mathrm{q}}^{\mathrm{p}} \end{bmatrix}+\begin{bmatrix} i_{\mathrm{d}}^{\mathrm{n'}} \\ i_{\mathrm{q}}^{\mathrm{n'}} \end{bmatrix}=\begin{bmatrix} I^{\mathrm{p}}+I^{\mathrm{n}}\cos(2\omega_{\mathrm{l}}\mathrm{t}+\varphi_{\mathrm{p}}+\varphi_{\mathrm{n}}) \\ -I^{\mathrm{n}}\sin(2\omega_{\mathrm{l}}\mathrm{t}+\varphi_{\mathrm{p}}+\varphi_{\mathrm{n}}) \end{bmatrix} \tag{20}$$

From the above equation, under the single grid-side current feedback control, due to the use of a PI regulator, it is impossible to implement static-free control of the AC component in (20). Therefore, a method based on the single grid-side current feedback control strategy cannot effectively inhibit an unbalanced input voltage on the input current.

The relationships among the virtual bus current i_{dc} and the input voltage, current positive sequence and negative sequence *dq* axis components are shown in (21):

$$\begin{aligned} i_{\mathrm{dc}}=&\frac{P(t)}{u_{\mathrm{dc}}}=\frac{3}{2}\frac{u_{\mathrm{d}}^{\mathrm{p}}i_{\mathrm{d}}^{\mathrm{p}}+u_{\mathrm{d}}^{\mathrm{n}}i_{\mathrm{d}}^{\mathrm{n}}}{u_{\mathrm{dc}}} \\ &+\frac{3}{2}\frac{1}{u_{\mathrm{dc}}}\left(u_{\mathrm{d}}^{\mathrm{n}}i_{\mathrm{d}}^{\mathrm{p}}\cos 2\omega_{\mathrm{l}}t-u_{\mathrm{d}}^{\mathrm{n}}i_{\mathrm{q}}^{\mathrm{p}}\sin 2\omega_{\mathrm{l}}t\right) \\ &+\frac{3}{2}\frac{1}{u_{\mathrm{dc}}}\left(u_{\mathrm{d}}^{\mathrm{p}}i_{\mathrm{d}}^{\mathrm{n}}\cos 2\omega_{\mathrm{l}}t+u_{\mathrm{d}}^{\mathrm{p}}i_{\mathrm{q}}^{\mathrm{n}}\sin 2\omega_{\mathrm{l}}t\right) \\ =&\bar{i}_{\mathrm{dc}}+\tilde{i}_{\mathrm{dc}}. \end{aligned} \tag{21}$$

where, $P(t)$ is the input active power, $u_{\mathrm{d}}^{\mathrm{p}}$ and $u_{\mathrm{q}}^{\mathrm{p}}$ are the projection of the positive sequence component of the input voltage under the positive sequence *dq* rotation axis, $u_{\mathrm{d}}^{\mathrm{n}}$ and $u_{\mathrm{q}}^{\mathrm{n}}$ are the projection of the negative sequence component of the input voltage under the negative sequence *dq* rotation axis, $i_{\mathrm{d}}^{\mathrm{p}}$ and $i_{\mathrm{q}}^{\mathrm{p}}$ are the projection of the positive sequence component of the input current under the positive sequence *dq* rotation axis, and $i_{\mathrm{d}}^{\mathrm{n}}$ and $i_{\mathrm{q}}^{\mathrm{n}}$ are the projection of the negative sequence component of the input current under the negative sequence *dq* rotation axis. $\bar{i}_{\mathrm{dc}}$ and $\tilde{i}_{\mathrm{dc}}$ are the amount of DC and ripple in the virtual dc bus current i_{dc}.

The expressions of the output voltage u_{o} and the compensation side voltage u_{cc} are shown in (22):

$$\begin{cases} u_{\mathrm{o}}=\xi_{\mathrm{m}}i_{\mathrm{dc}}Z_{\mathrm{L}}=i_{\mathrm{dc}}M_{\mathrm{m}}\cos(\omega_{\mathrm{o}}t+\varphi_{\mathrm{o}})\left|Z_{\mathrm{L}}\right| \\ u_{\mathrm{cc}}=\dfrac{1}{C_{\mathrm{c}}}\int i_{\mathrm{cc}}\mathrm{d}t=-\dfrac{i_{\mathrm{dc}}M_{\mathrm{c}}}{C_{\mathrm{c}}\omega_{\mathrm{o}}}\cos(\omega_{\mathrm{o}}t+\varphi_{\mathrm{c}}). \end{cases} \tag{22}$$

From (21) it can be seen that if the system unbalance is small, if $u_{\mathrm{d}}^{\mathrm{n}}$ □ $u_{\mathrm{d}}^{\mathrm{p}}$, then $i_{\mathrm{dc}}\approx\bar{i}_{\mathrm{dc}}$. In addition, it is possible to ignore the effect of the virtual bus current twice the input frequency harmonics on the output voltage. When the imbalance is large, the harmonics contained in i_{dc} distort the output. If the above control strategy is still used at this time, (21) and (22) show that the output voltage contains the

harmonics of $2\omega_i$-ω_o and $2\omega_i$+ω_o, respectively.

B. Method of Suppressing Double Frequency Pulsation in Input Active Power Under an Unbalanced Input

Assuming that input unbalanced voltage contains only positive and negative sequence components, the complex vector expression under the *dq* rotation coordinate of the input voltage and current is:

$$\begin{cases} U_{\mathrm{dqs}} = e^{j\omega_i t}(u_{\mathrm{d}}^{\mathrm{p}} + ju_{\mathrm{q}}^{\mathrm{p}}) + e^{-j\omega_i t}(u_{\mathrm{d}}^{\mathrm{n}} + ju_{\mathrm{q}}^{\mathrm{n}}), \\ I_{\mathrm{dqs}} = e^{j\omega_i t}(i_{\mathrm{d}}^{\mathrm{p}} + ji_{\mathrm{q}}^{\mathrm{p}}) + e^{-j\omega_i t}(i_{\mathrm{d}}^{\mathrm{n}} + ji_{\mathrm{q}}^{\mathrm{n}}). \end{cases} \tag{23}$$

The relationships among the system apparent power S, the active power $P(t)$, and the reactive power $Q(t)$ are:

$$S = U_{\mathrm{dqs}} \times \overline{I_{\mathrm{dqs}}} = P(t) + jQ(t) \tag{24}$$

where, $\overline{I_{\mathrm{dqs}}}$ is the conjugated plural form of I_{dqs}. In addition:

$$\begin{cases} P(t) = \bar{P}(t) + \tilde{P}(t) = P_{\mathrm{o}} + P_{\mathrm{c}}\cos(2\omega_i t) + P_{\mathrm{s}}\sin(2\omega_i t) \\ Q(t) = \bar{Q}(t) + \tilde{Q}(t) = Q_{\mathrm{o}} + Q_{\mathrm{c}}\cos(2\omega_i t) + Q_{\mathrm{s}}\sin(2\omega_i t) \end{cases} \tag{25}$$

where, P_{o} and Q_{o} are the constant terms of the active power and reactive power, $\bar{P}(t)$ and $\tilde{P}(t)$ are the steady and fluctuating amounts of active power, $\bar{Q}(t)$ and $\tilde{Q}(t)$ are the steady and fluctuating amounts of reactive power, and P_{c} and P_{s} are the amplitudes of the active power cosine and sinusoidal ripple, respectively. Q_{c} and Q_{s} are the amplitudes of the reactive power cosine and sinusoidal ripple, respectively.

From (25), it can be seen that the pulsation component $\tilde{P}(t) \neq 0$ in the active power generates a double-frequency input ripple on the virtual dc bus. If the reactive power $Q(t) \neq 0$, the unity power factor cannot be achieved on the input side. Since the input and output of the system are directly connected, the input active power ripple also affects the output side. Therefore, it is impossible to reduce the influence of the unbalance on the output via absorbing harmonics by increasing the output filter capacitance in the PWM rectification control, since there is no large-capacity energy storage unit in the 3-1MC topology.

Therefore, in order to suppress the influence of the input active power secondary ripple on the input current and output voltage, the control system is designed to control the instantaneous active power 2nd harmonic component amplitude in (25) under the condition that the system output active power P_{o} is determined by the output of the outer loop regulator. The values P_{c}, P_{s}, and instantaneous reactive power dc component amplitude Q_{o} are zero. In this paper, independent control of the four control variables is implemented in the positive and negative sequence *dq* coordinate system of the input current, in order to suppress the double-frequency harmonics of the active power input at the grid side. The current decoupling inner loop control object expression is:

$$\begin{bmatrix} i_{\mathrm{d}}^{\mathrm{p}*} \\ i_{\mathrm{q}}^{\mathrm{p}*} \\ i_{\mathrm{d}}^{\mathrm{n}*} \\ i_{\mathrm{q}}^{\mathrm{n}*} \end{bmatrix} = \frac{\frac{2}{3}P_{\mathrm{o}}}{\left(u_{\mathrm{d}}^{\mathrm{p}}\right)^2 - \left(u_{\mathrm{d}}^{\mathrm{n}}\right)^2} \times \begin{bmatrix} u_{\mathrm{d}}^{\mathrm{p}} \\ u_{\mathrm{q}}^{\mathrm{p}} \\ -u_{\mathrm{d}}^{\mathrm{n}} \\ -u_{\mathrm{q}}^{\mathrm{n}} \end{bmatrix} = \frac{2P_{\mathrm{o}}}{3D} \times \begin{bmatrix} u_{\mathrm{d}}^{\mathrm{p}} \\ u_{\mathrm{q}}^{\mathrm{p}} \\ -u_{\mathrm{d}}^{\mathrm{n}} \\ -u_{\mathrm{q}}^{\mathrm{n}} \end{bmatrix} \tag{26}$$

where, $i_{\mathrm{d}}^{\mathrm{p}*}$、$i_{\mathrm{q}}^{\mathrm{p}*}$、$i_{\mathrm{d}}^{\mathrm{n}*}$、$i_{\mathrm{q}}^{\mathrm{n}*}$ are the current commands for the input current positive and negative sequence components in the positive and negative sequence *dq* rotation axes.

C. Balanced Input Controller Design Based on a Lyapunov Function in the dq Axis Coordinates

The input voltage and current under a three-phase balanced input, and the expression in the *dq* axis coordinate system of the converter input voltage are:

$$\begin{cases} L\dfrac{di_{\mathrm{d}}}{dt} = u_{\mathrm{d}} - Ri_{\mathrm{d}} + \omega_i L i_{\mathrm{q}} - u_{\mathrm{d}}' \\ L\dfrac{di_{\mathrm{q}}}{dt} = u_{\mathrm{q}} - Ri_{\mathrm{q}} - \omega_i L i_{\mathrm{d}} - u_{\mathrm{q}}' \end{cases} \tag{27}$$

where, i_{d} and i_{q} denote the components of the input current on the *dq* axis. u_{d}' and u_{q}' denote the components of the input voltage of the matrix converter on the *dq* axis.

The error functions e_1 and e_2 defined in the input three-phase current *dq* axis coordinate system are:

$$\begin{cases} e_1 = i_{\mathrm{d}}^* - i_{\mathrm{d}} \\ e_2 = i_{\mathrm{q}}^* - i_{\mathrm{q}} \end{cases} \tag{28}$$

where, i_{d}^* and i_{q}^* are the current *dq* axis component settings.

Take the positive definite Lyapunov function expression u_1 as:

$$u_1 = \frac{1}{2}(e_1^2 + e_2^2) \tag{29}$$

The derivative of the above formula is as follows:

$$\dot{u}_1 = e_1\dot{e}_1 + e_2\dot{e}_2 \tag{30}$$

Substituting Equ. (27) into (30) yields:

$$\begin{aligned} \dot{u}_1 = e_1(\dot{i}_{\mathrm{d}}^* - \dot{i}_{\mathrm{d}}) + e_2(\dot{i}_{\mathrm{q}}^* - \dot{i}_{\mathrm{q}}) = e_1\left[\dot{i}_{\mathrm{d}}^* - (\frac{1}{L}u_{\mathrm{d}} - \frac{R}{L}i_{\mathrm{d}} + \omega_i i_{\mathrm{q}} - \frac{1}{L}u_{\mathrm{d}}')\right] \\ + e_2\left[\dot{i}_{\mathrm{q}}^* - (\frac{1}{L}u_{\mathrm{q}} - \frac{R}{L}i_{\mathrm{q}} - \omega_i i_{\mathrm{d}} - \frac{1}{L}u_{\mathrm{q}}')\right] \end{aligned} \tag{31}$$

In order to make the system stable, the Lyapunov function needs to be a positive definite function. The coefficients are chosen as $\lambda_1 > 0$ and $\lambda_2 > 0$. From the above formula, the

expression $\dot{u}_1 = -\lambda_1 e_1^2 - \lambda_2 e_2^2 < 0$ is obtained. Then it is possible to derive:

$$\begin{cases} i_{\mathrm{d}}^{*} - (\frac{1}{L}u_{\mathrm{d}} - \frac{R}{L}i_{\mathrm{d}} + \omega_{\mathrm{i}} i_{\mathrm{q}} - \frac{1}{L}u_{\mathrm{d}}^{'}) = -\lambda_1 e_1 \\ i_{\mathrm{q}}^{*} - (\frac{1}{L}u_{\mathrm{q}} - \frac{R}{L}i_{\mathrm{q}} - \omega_{\mathrm{i}} i_{\mathrm{d}} - \frac{1}{L}u_{\mathrm{q}}^{'}) = -\lambda_2 e_2 \end{cases} \tag{32}$$

From the above formula, the target control quantity expressions of $u_{\mathrm{d}}^{'}$ and $u_{\mathrm{q}}^{'}$ for the input side voltage of the matrix converter under the *dq* coordinate system are as follows:

$$\begin{cases} u_{\mathrm{d}}^{'} = -L\lambda_1 e_1 - Li_{\mathrm{d}}^{*} + u_{\mathrm{d}} - R_{\mathrm{i}} i_{\mathrm{d}} + \omega_{\mathrm{i}} L i_{\mathrm{q}} \\ u_{\mathrm{q}}^{'} = -L\lambda_2 e_2 - Li_{\mathrm{q}}^{*} + u_{\mathrm{q}} + R_{\mathrm{i}} i_{\mathrm{q}} - \omega_{\mathrm{i}} L i_{\mathrm{d}} \end{cases} \tag{33}$$

D. Realization of a 3-1MC Control Strategy Based on a Lyapunov Function under an Unbalanced Input

According to Equ. (28), the current error expression under an unbalanced input on the input side positive and negative sequence axes is:

$$\begin{cases} e_1^{'} = i_{\mathrm{d}}^{\mathrm{p}*} - i_{\mathrm{d}}^{\mathrm{p}} \quad e_2^{'} = i_{\mathrm{q}}^{\mathrm{p}*} - i_{\mathrm{q}}^{\mathrm{p}} \\ e_3^{'} = i_{\mathrm{d}}^{\mathrm{n}*} - i_{\mathrm{d}}^{\mathrm{n}} \quad e_4^{'} = i_{\mathrm{q}}^{\mathrm{n}*} - i_{\mathrm{q}}^{\mathrm{n}} \end{cases} \tag{34}$$

where, $e_1^{'}$ and $e_2^{'}$ are current error functions under the positive sequence axis, and $e_3^{'}$ and $e_4^{'}$ are current error functions under the negative sequence axis.

When the three-phase input is unbalanced, the positive and negative sequence *dq* axis voltages $u_{\mathrm{d}}^{\mathrm{p}}$、$u_{\mathrm{q}}^{\mathrm{p}}$、$u_{\mathrm{d}}^{\mathrm{n}}$ and $u_{\mathrm{q}}^{\mathrm{n}}$ on the converter side are used as control variables, and the positive and negative sequence *dq* axis current components $i_{\mathrm{d}}^{\mathrm{p}}$、$i_{\mathrm{q}}^{\mathrm{p}}$、$i_{\mathrm{d}}^{\mathrm{n}}$ and $i_{\mathrm{q}}^{\mathrm{n}}$ on the grid side are used as control objects. The 3-1MC input current is decoupled and the positive and negative sequence *dq* axis controllers independently control the *dq* axis component of the input current. This is done to control the input side current waveform and power factor. Since the current loop adopts a regular pattern based on a Lyapunov function, according to the feed-forward decoupling control law, and in combination with the expression of the target control quantity function under the equilibrium condition represented by (33), the conversion under the unbalanced condition can be obtained. The equations of the control commands for the positive and negative sequence voltages $u_{\mathrm{d}}^{\mathrm{p}*}$、$u_{\mathrm{q}}^{\mathrm{p}*}$、$u_{\mathrm{d}}^{\mathrm{n}*}$ and $u_{\mathrm{q}}^{\mathrm{n}*}$ at the input side of the converter under unbalanced conditions are shown in (35) and (36):

$$\begin{cases} u_{\mathrm{d}}^{\mathrm{p}*} = -L\lambda_{12} e_1^{'} - Li_{\mathrm{d}}^{\mathrm{p}*'} + u_{\mathrm{d}}^{\mathrm{p}} - Ri_{\mathrm{d}}^{\mathrm{p}} + \omega_{\mathrm{i}} L i_{\mathrm{q}}^{\mathrm{p}} \\ u_{\mathrm{q}}^{\mathrm{p}*} = -L\lambda_{12} e_2^{'} - Li_{\mathrm{q}}^{\mathrm{p}*'} + u_{\mathrm{q}}^{\mathrm{p}} + Ri_{\mathrm{q}}^{\mathrm{p}} - \omega_{\mathrm{i}} L i_{\mathrm{d}}^{\mathrm{p}} \end{cases} \tag{35}$$

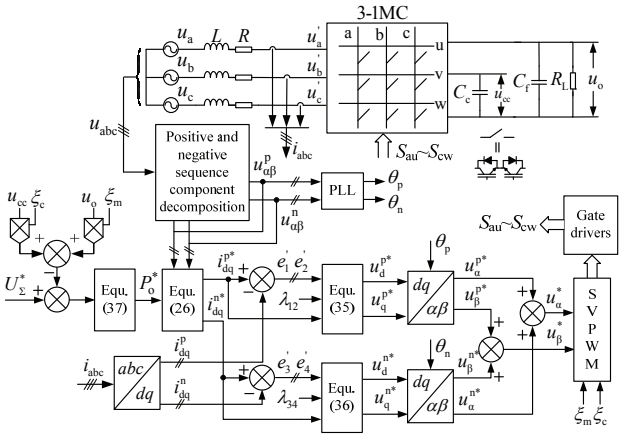

Fig. 6. Dual current decoupling closed-loop control strategy block diagram based on a Lyapunov function.

$$\begin{cases} u_{\mathrm{d}}^{\mathrm{n}*} = -L\lambda_{34} e_3^{'} - Li_{\mathrm{d}}^{\mathrm{n}*} + u_{\mathrm{d}}^{\mathrm{n}} + Ri_{\mathrm{d}}^{\mathrm{n}} - \omega_{\mathrm{i}} L i_{\mathrm{q}}^{\mathrm{n}} \\ u_{\mathrm{q}}^{\mathrm{n}*} = -L\lambda_{34} e_4^{'} - Li_{\mathrm{q}}^{\mathrm{n}*} + u_{\mathrm{q}}^{\mathrm{n}} - Ri_{\mathrm{q}}^{\mathrm{n}} + \omega_{\mathrm{i}} L i_{\mathrm{d}}^{\mathrm{n}} \end{cases} \tag{36}$$

The outer loop control often uses an output side voltage amplitude closed loop. However, this method requires a phase locked loop, which increases the difficulty and computational complexity. This study uses the output-side and compensation side voltage weighted synthesis as the feedback value, and the outer loop is output by the PI regulator as the constant component command value P_{o}^{*} of the output active power. Its expression is shown in (37), and a 3-1MC control block diagram is shown in Fig. 6.

$$P_{\mathrm{o}}^{*} = \left(k_{\mathrm{p}} + \frac{k_{\mathrm{i}}}{s}\right)\left[U_{\Sigma}^{*} - (u_{\mathrm{o}}\xi_{\mathrm{m}} + u_{\mathrm{cc}}\xi_{\mathrm{c}})\right] \tag{37}$$

where, k_{p} and k_{i} are the proportional and integral parameters in the outer loop PI regulator.

IV. SIMULATION RESULTS

In order to verify the effectiveness of the proposed control strategy, simulations have been carried out using MATLAB/ Simulink. The system simulation parameters are set as follows:

1) Three-phase unbalanced voltage $u_{\mathrm{a}} = 18\sqrt{2}, u_{\mathrm{b}} = 15\sqrt{2}$, and $u_{\mathrm{c}} = 12\sqrt{2}$.

2) Input frequency $f_{\mathrm{i}} = 50\mathrm{Hz}$.

3) Input inductance parameters $L = 3\mathrm{mH}$ and R=0.2Ω.

4) Output voltage amplitude $U_{\mathrm{o}} = 110\sqrt{2}\mathrm{V}$.

5) Output frequency $f_{\mathrm{o}} = 60\mathrm{Hz}$.

6) Output filter parameter $C_{\mathrm{f}} = 4.4\mathrm{uF}$.

7) Switching frequency $f_{\mathrm{s}} = 10\mathrm{kHz}$.

Fig. 7 shows simulation waveforms of the three-phase input current and output voltage using a single grid-side current

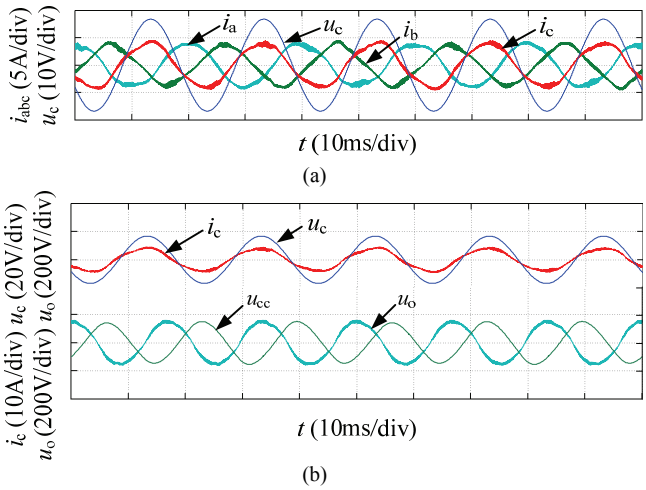

Fig. 7. Simulation results obtained using a single grid-side current feedback loop under an unbalanced input voltage: (a) Three phase current waveforms of the input side; (b) Steady-state simulation waveforms of the input voltage current u_c, i_c and the output voltage u_o, u_{cc}.

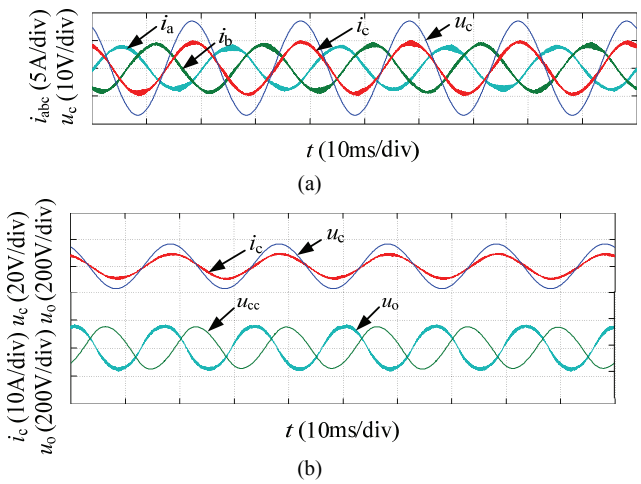

Fig. 8. Simulation results of the double current decoupled closed-loop strategy: (a) Input steady-state simulation waveforms of the three-phase current i_{abc}; (b) Steady-state simulation waveforms of the input voltage current u_c, i_c and the output voltage u_o, u_{cc}.

feedback loop under an unbalanced input voltage. From the simulation waveforms, it can be seen that the three-phase input current waveform distortions are severe, and that the total harmonic distortion (THD) of the three-phase input current i_{abc} are 8.12%, 8.67% and 8.18%. In addition, the unbalanced voltage also affects the output voltage u_o. The THD of the output voltage u_o is 4.62%.

Fig. 8 shows the dual-current decoupling based on a Lyapunov function to the inner loop, the output side voltage and the compensation side voltage weighted synthesis amount as outer loop simulation waveforms. According to Fig. 8(a), the input steady-state current waveforms at the input unbalanced voltage are good, and the phase difference between the output side and the compensation side satisfies the requirements of Equ. (10). When compared with the input current simulation results using single grid-side current feedback control (Fig. 7), the quality of the three-phase input current i_{abc} and the output voltage u_o waveforms under the proposed control strategy are improved, and the respective THD values of the input currents are improved. The THD values of the input currents i_{abc} are: 4.63%, 3.74% and 3.55%. The THD of the output voltage u_o is 4.16%.

V. Experimental Results and Analysis

In order to verify the effectiveness of the proposed control strategy, a prototype of the proposed 3-1MC based on four-step commutation is built with a DSP28335+CPLD as the main control core. The voltage and current samples in the prototype are measured by Hall sensors VSM025A and CSM025, the optocoupler is driven by TLP250, the power circuit is composed of 18 IGBTs of 1MBH60D-100, and the bidirectional switch is composed of two 1MBH60D-100. The system experiment parameters are set as follows:

1) Three-phase unbalanced voltages $u_a = 18\sqrt{2}$, $u_b = 15\sqrt{2}$, and $u_c = 12\sqrt{2}$.

2) Input frequency $f_i = 50\text{Hz}$.

3) Input inductance parameters $L = 3\text{mH}$ and R=0.2Ω.

4) Output voltage amplitude $U_o = 110\sqrt{2}\text{V}$.

5) Output frequency $f_o = 60\text{Hz}$.

6) Output filter parameter $C_f = 4.4\text{uF}$.

7) Switching frequency $f_s = 10\text{kHz}$.

8) Four-step commutation time 2.7us.

Fig. 9 shows steady-state experimental waveforms of the input currents i_{abc} for the single grid-side current feedback control strategy under input three-phase voltage unbalanced conditions. From this figure, it can be seen that the control strategy cannot effectively suppress the influence of the unbalanced voltage on the input current and output voltage. These three-phase input current waveforms show obvious asymmetry and distortion. The THD values of the three-phase input current i_{abc} under the single grid-side current feedback control strategy are: 11.8%, 13.18% and 12.19%. The THD value of the output voltage u_o is 5.95%. This result is consistent with the simulation analysis in Fig. 7.

Fig. 10 shows three-phase steady-state input current and output voltage waveforms under the input unbalanced control strategy proposed in this paper. When compared with Fig. 9, the low-frequency harmonics in the three-phase input current are significantly suppressed and the input performance is improved. Additionally, the steady-state output is good. The THD values of the three-phase input current i_{abc} under the control strategy proposed in this paper are: 7.71%, 6.92%, and 6.64%. The THD value of the output voltage u_o is 5.48%.

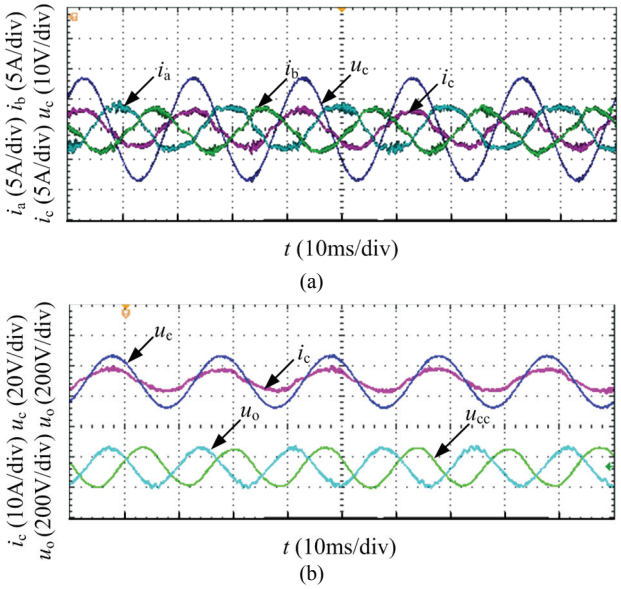

Fig. 9. Steady-state experimental waveforms under unbalanced input based on single grid-side current feedback control: (a) Input phase voltage u_c and three-phase current i_{abc} steady-state experiment waveforms; (b) Input voltage current u_c, i_c and output voltage u_o, u_{cc} steady-state experiment waveforms.

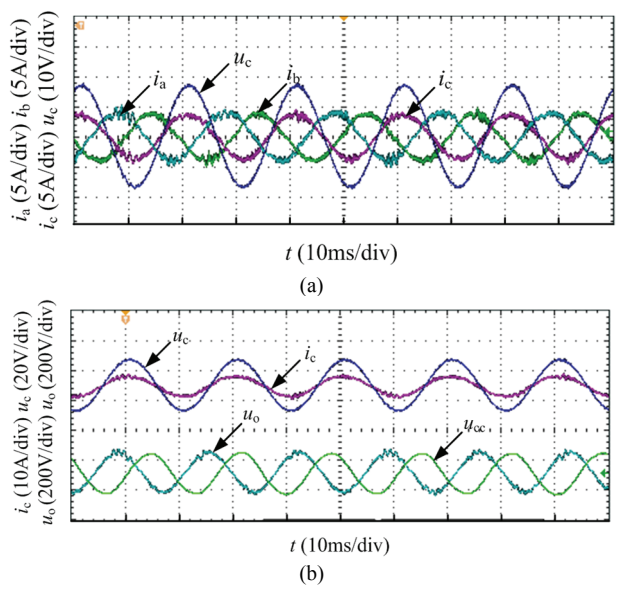

Fig. 10. Lyapunov-based steady-state experiment waveforms of the unbalanced closed-loop strategy with double current decoupling: (a) Input phase voltage u_c and three-phase current i_{abc} steady-state experiment waveforms; (b) Input voltage current u_c, i_c and output voltage u_o, u_{cc} steady-state experiment waveforms.

Fig. 11 shows a transient process in which the system switches from a balanced input to unbalanced conditions under the unbalanced control strategy based on a Lyapunov function, in which the RMS of the phase C voltage u_c is suddenly reduced from 18V to 12V. From this figure, it can be seen that the output voltage u_o, and the input currents i_b and i_c can all reach a stable state quickly, and that the dynamic response process is very short and there is no obvious oscillation, which indicates that the control strategy proposed in this paper can effectively suppress unbalanced input current and output voltage.

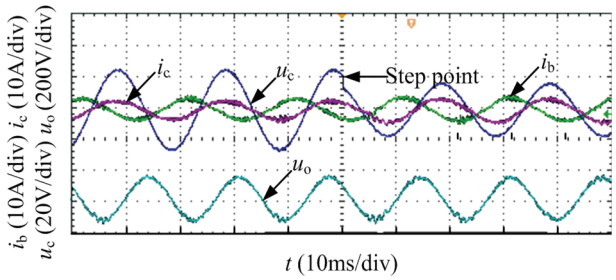

Fig. 11. Switching from input voltage to unbalanced dynamic experimental waveforms based on Lyapunov function and dual current decoupling closed-loop strategy.

VI. Conclusion

This paper studied a 3-1MC topology, which can suppress the effect of output ripple on input performance. The principle of pulsating power absorption, the implementation process, and the effect on the system voltage transmission rate were analyzed in detail. For a 3-1MC without large capacity storage capacitors, input asymmetry can easily cause system performance degradation. This paper proposed a 3-1MC asymmetric control strategy based on a Lyapunov function in positive and negative sequence dual coordinates. Finally, a system simulation model was established and an experimental platform was built to verify the effectiveness and feasibility of the proposed control strategy. Experimental results showed that under an asymmetric input, when compared with the traditional single grid-side current feedback control strategy, the input and output performances based on the proposed control strategy were greatly improved and that the input side power factor was high. At the same time, experimental results of the transient response showed that the input and output response time was short and without obvious oscillation. The above results show that the proposed control strategy has the advantage of convenient debugging. They also show that it has the ability to eliminate the impact of output ripple power and input asymmetry on system performance, and improve the practicality of the studied topology.

Acknowledgment

This paper is funded by the following fund: The National Natural Science Foundation of China (Fund number U1233127); Huzhou Natural Science Fund Project (Fund number 2017YZ09).

REFERENCES

[1] L. Empringham, J. W. Kolar, J. Rodriguez, P. W. Wheeler, and J. C. Clare, "Technological issues and industrial application of matrix converters: A review," *IEEE Trans. Ind. Electron.*, Vol. 60, No. 10, pp. 4260-4271, Oct. 2013.

[2] D. Varajão, E. A. Rui, L. M. Miranda, and J. Lopes, "Modulation strategy for a single-stage bidirectional and isolated AC-DC matrix converter for energy storage systems," *IEEE Trans. Ind. Electron.*, Vol. 65, No. 4, pp. 3458-3468, Apr. 2018.

[3] F. Fang and Y. W. Li, "Modulation and control method for bidirectional isolated AC/DC matrix based converter in hybrid AC/DC microgrid," in *Energy Conversion Congress and Exposition*, pp. 37-43, 2017.

[4] K. Inaba, H. Koizumi, K. Ishibashi, and Y. Nishida, "Operation of three-phase to single-phase matrix converter with power decoupling inductor for distribution network at zero power factor," in *Future Energy Electronics Conference*, pp. 1-6, 2015.

[5] F. P. Kusumah, S. Vuorsalo, and J. Kyyra, "Components selection of a direct three-phase to single-phase AC/AC converter for a contactless electric vehicle charger," in *European Conference on Power Electronics and Applications*, pp. 1-10, 2016.

[6] E. Karaman, M. Farasat, F. Niu, and A. M. Trzynadlowski, "Three-phase to single-phase super-sparse matrix converters," in *Twenty-Seventh IEEE Applied Power Electronics Conference and Exposition*, pp. 1061-1066, 2012.

[7] C. Gu, H. S. Krishnamoorthy, P. N. Enjeti, Z. Zheng, and Y. Li, "A medium-voltage matrix converter topology for wind power conversion with medium frequency transformers," *J. Power Electron.*, Vol. 14, No. 6, pp. 1166-1177, Nov. 2014.

[8] N. Nguyen-Quang, D. A. Stone, C. M. Bingham, and M. P. Foster, "A three-phase to single-phase matrix converter for high-frequency induction heating," in *European Conference on Power Electronics and Application*, pp. 1-10, 2009.

[9] Y. Ohnuma and J. I. Itoh, "Novel control strategy for single-phase to three-phase power converter using an active buffer," *European Conference on Power Electronics and Applications*, pp. 1-10, 2009.

[10] Y. Miura, T. Amano, and T. Ise, "Operating characteristics of a three-phase to single-phase matrix converter with hybrid control scheme of power compensation and modulation applied to gas engine cogeneration system," in *European Conference on Power Electronics and Applications*, Vol. 8, pp. 1-10, 2011.

[11] S. Chen, H. Ge, Zhang W, and S. Lu, "A control strategy based on small signal model for three-phase to single-phase matrix converters," *J. Power Electron.*, Vol. 15, No. 6, pp. 1456-1467, Nov. 2015.

[12] Y. Liu, W. Liang, B. Ge, H. Abu-Rub, and N. Nie, "Quasi-Z-source three-to-single-phase matrix converter and ripple power compensation based on model predictive control," *IEEE Trans. Ind. Electron.*, 2017, Vol. 65, No. 6, pp. 5146-5156, Jun. 2018.

[13] Y. Yan, H. An, T. Shi, and C. Xia, "Improved double line voltage synthesis of matrix converter for input current enhancement under unbalanced power supply," *IET Power Electron.*, Vol. 6, No. 4, pp. 798-808, Apr. 2013.

[14] M. Hamouda, H. F. Blanchett, and K. Al-Haddad, "Unity power factor operation of indirect matrix converter tied to unbalanced grid," *IEEE Trans. Power Electron.*, Vol. 31, No. 2, pp. 1095-1107, Feb. 2016.

[15] J. Lei, B. Zhou, J. Bian, J. Wei, and Y. Zhu, "Feedback control strategy to eliminate the input current harmonics of matrix converter under unbalanced input voltages," *IEEE Trans. Power Electron.*, Vol. 32, No.1, pp. 878-888, Jan. 2016.

[16] H. S. Song and K. Nam, "Dual current control scheme for PWM converter under unbalanced input voltage conditions," *IEEE Trans. Ind. Electron.*, Vol. 46, No. 5, pp. 953-959, Oct. 1999.

[17] M. Salimi and A. Zakipour, "Lyapunov based adaptive-robust control of the non-minimum phase DC-DC converters using input–output linearization," *J. Power Electron.*, Vol. 15, No. 6, pp. 1577-1583, Nov. 2015.

[18] M. Kabalan, P. Singh, and D. Niebur, "Large signal lyapunov-based stability studies in microgrids: A review," *IEEE Trans. Smart Grid*, Vol. 8, No. 5, pp. 2287-2295, Sep. 2017.

Yu-xiang Xu was born in Zhejiang, China, in 1981. He received his B.S. and M.S. degrees in Mechanical Engineering from the Zhejiang University of Technology (ZJUT), Hangzhou, China, in 2004 and 2008, respectively. He is presently working towards his Ph.D. degree in Electric Machines and Electric Apparatus from the Nanjing University of Aeronautics and Astronautics (NUAA), Nanjing, China. His current research interests include matrix converters and digital control of power converters.

Hong-juan Ge was born in Jiangsu, China, in 1966. She received her B.S. and M.S. degrees in Electrical Engineering from Southeast University, Nanjing, China, in 1985 and 1988, respectively; and her Ph.D. degree in Electric Machines and Electric Apparatus from the Nanjing University of Aeronautics and Astronautics (NUAA), Nanjing, China, in 2006. Her current research interests include space-vector control of PWM, AC-AC converters, and airworthiness technology.

Hai Guo received his M.S. degree from the Hefei University of Technology, Hefei, China, in 2009. He is presently working towards his Ph.D. degree in the College of Automation Engineering, Nanjing University of Aeronautics and Astronautics (NUAA), Nanjing, China. Since 2009, he has been working as an Associate Professor at the Anhui University of Science and Technology, Huainan, China. His current research interests include matrix converters, power electronics, and automatic control technologies.